Front. Phys. 13(5), 134101 (2018)
https://doi.org/10.1007/s11467-018-0764-4

RESEARCH ARTICLE

Perfect invisibility concentrator with simplified material parameters

Meng-Yin Zhou[1], Lin Xu[1], Lu-Chan Zhang[1], Jiang Wu[2], Yan-Bo Li[2,†], Huan-Yang Chen[1,‡]

[1] *Institute of Electromagnetics and Acoustics and Department of Electronic Science, Xiamen University, Xiamen 361005, China*
[2] *Institute of Fundamental and Frontier Sciences, University of Electronic Science and Technology of China, Chengdu 610054, China*
Corresponding authors. E-mail: †yanboli@uestc.edu.cn, ‡kenyon@xmu.edu.cn
Received April 17, 2018; accepted May 10, 2018

We present a series of invisibility concentrators with simplified material parameters beyond transformation optics. One of them can achieve the perfect invisible effect at frequencies of Fabry–Pérot resonances, while others have very small scattering. The required materials are feasible in practice. Analytical calculations and numerical simulations confirm the functionalities of these devices.

Keywords perfect-invisibility concentrator, simplified material parameters, Fabry–Pérot resonances, scattering cross section

PACS numbers 41.20.Jb, 42.25.Bs, 42.25.Fx

1 Introduction

From a geometrical perspective, transformation optics (TO) [1, 2] theoretically show us how light propagates in a continuous medium, which is equivalent to curved space [3–5]. In the past decade, TO has been implemented using metamaterials, revealing its powerful ability to design versatile optical devices, such as invisibility cloaks [1, 2], rotators [6], carpet cloaks [7, 8], illusion devices [9–11], and concentrators [12, 13]. The required material parameters for TO are usually inhomogeneous and anisotropic tensors or even have some singularities [1, 2]. In practical experiments, simplified material parameters are introduced for fabrication, such as the invisibility cloak [14] and the rotator [15] realized in microwaves. After simplification, the perfect performance of the invisibility and rotation is compromised [15, 16].

Recently, by simplification of the optical void medium [10, 17] with Fabry–Pérot resonances (FPs), a prototype of a concentrator was realized to achieve concentration of electromagnetic waves [18]. Such a prototype designed with simplified material parameters has small scatterings at multiple frequencies of FPs and thus cannot be treated as a perfect-invisibility device.

In this letter, we present a concentrator with simplified material parameters, which has no scattering at frequencies of FPs. Therefore, such a concentrator cannot be detected by outside observers, making it a perfect invisibility device. Furthermore, we find that a series of invisibility devices with other simplified material parameters are almost perfect, with very small scattering. We will introduce two of these in detail. All of these simplified material parameters are more feasible in practice. Analytical calculations and numerical simulations confirm the functionalities of these concentrators.

Via coordinate transformation of the concentrator in the two-dimensional space, we can compress the circular region with radius R_1' in the virtual space shown in Fig. 1(a) to the circular region with radius R_2 in the physical space shown in Fig. 1(b), while keeping the region outside radius R_1 unchanged. The region between the radii R_1' and R_1 in Fig. 1(a) is mapped to that between the radii R_1 and R_2 in Fig. 1(b). The whole coordinate transformation between the virtual space with the (r', θ') coordinate system and the physical space with the (r, θ) coordinate system is written as follows:

$$\begin{cases} r = r', & (r' > R_1) \\ r = R_2 + \dfrac{R_1 - R_2}{R_1 - R_1'}(r' - R_1'), & (R_1' \le r' \le R_1) \\ r = \dfrac{R_2}{R_1'} r', & (r' < R_1') \end{cases} . \quad (1)$$

The virtual space is vacuum, and its permittivity and

permeability are ε_0 and μ_0, respectively. The permittivity and permeability tensors of required materials in physical space are obtained from Eq. (1) via TO, as follows:

$$\begin{cases} \dfrac{\overleftrightarrow{\varepsilon_1}}{\varepsilon_0} = \dfrac{\overleftrightarrow{\mu_1}}{\mu_0} = \begin{bmatrix} \dfrac{R_1 - R_2}{R_1 - R_1'}\dfrac{r'}{r} & 0 & 0 \\ 0 & \dfrac{R_1 - R_1'}{R_1 - R_2}\dfrac{r}{r'} & 0 \\ 0 & 0 & \dfrac{R_1 - R_1'}{R_1 - R_2}\dfrac{r}{r'} \end{bmatrix}, & R_2 \le r \le R_1, \\ \dfrac{\overleftrightarrow{\varepsilon_2}}{\varepsilon_0} = \dfrac{\overleftrightarrow{\mu_2}}{\mu_0} = \begin{bmatrix} 1 & 0 & 0 \\ 0 & 1 & 0 \\ 0 & 0 & \left(\dfrac{R_1'}{R_2}\right)^2 \end{bmatrix}, & r < R_2. \end{cases} \tag{2}$$

For the region outside radius R_1, the permittivity and permeability are unchanged, as shown in Fig. 1(b).

We consider the special scenario where radius R_1' approaches radius R_1. Then, Eq. (2) asymptotically approaches

$$\begin{cases} \dfrac{\overleftrightarrow{\varepsilon_1}}{\varepsilon_0} = \dfrac{\overleftrightarrow{\mu_1}}{\mu_0} = \begin{bmatrix} \infty & 0 & 0 \\ 0 & 0 & 0 \\ 0 & 0 & 0 \end{bmatrix}, & R_2 \le r \le R_1, \\ \dfrac{\overleftrightarrow{\varepsilon_2}}{\varepsilon_0} = \dfrac{\overleftrightarrow{\mu_2}}{\mu_0} = \begin{bmatrix} 1 & 0 & 0 \\ 0 & 1 & 0 \\ 0 & 0 & \left(\dfrac{R_1}{R_2}\right)^2 \end{bmatrix}, & r < R_2. \end{cases} \tag{3}$$

In this situation, it appears that the region between the radii R_1 and R_2 in Fig. 1(b) has no place to be mapped from. The materials in this region have singularity, as shown in Eq. (3), which is usually called an optical void medium [10]. In this region, a light ray (in red) can only propagate along the r direction. Because the effective refractive index is zero along such an optical path, there is no phase change. For the other direction, i.e., the θ direction, the effective refractive index is infinity, which prevents the propagation of light in such a direction. In the regions outside radius R_1 and inside radius R_2, the effective refractive index is 1 and R_1/R_2, respectively. In experiments, the optical void medium is not easy to fabricate for finite frequencies (there are several designs for zero frequency in controlling static magnetic fields [19–23]).

Recently, simplification of the optical void medium with FPs has been proposed to achieve the concentration effect in the transverse-magnetic mode (TM mode) [18], only considering the components (E_r, E_θ, H_z) in the electromagnetic parameters of $(\varepsilon_r', \varepsilon_\theta', \mu_z')$. The main feature of this simplification is to keep the effective refractive index outside radius R_1 and inside radius R_2 unchanged, while continuously changing the effective refractive index from radius R_1 to radius R_2. The procedure of simplification reduces the parameters in Eq. (3) as follows:

$$\begin{aligned} (\varepsilon_r', \varepsilon_\theta', \mu_z') &= (\infty, \alpha(r), \beta(r)), \quad R_2 < r < R_1, \\ (\varepsilon_2', u_2') &= (\alpha(R_2)\varepsilon_0, \beta(R_2)u_0), \quad r < R_2, \end{aligned} \tag{4}$$

where $\alpha(r)$ and $\beta(r)$ are functions of r, which only depend on $R_2 \le r \le R_1$. They are chosen such that the effective refractive index along the r direction ($n_r(r) = \sqrt{\alpha(r)\beta(r)}$) is continuous at both radii R_1 and R_2 for the TM mode. The effective refractive index along the r direction inside radius R_2 is kept as $n_r(r) = \sqrt{\alpha(R_2)\beta(R_2)} = R_1/R_2$. In this simplification, the effective refractive index along the r direction changes continuously in the physical space, as shown in the contour plot of Fig. 1(c). Once the effective refractive index along the r direction is no longer zero, there is an additional optical path. Thus, there exists a phase change along the r direction, as shown schematically by the wave line (in red) between the radii R_1 and R_2.

Thus far, we have obtained a model of the concentrator with the simplified material parameters in Eq. (4) for the TM mode, as shown in Fig. 1(c). In a previous work [18], $(\varepsilon_r', \varepsilon_\theta', \mu_z')$ are chosen to be $(\infty, (3-r)^2, 1)$ to demonstrate the concentration effect and invisibility at frequencies of FPs. Nevertheless, the invisibility effect of such a concentrator is not perfect, and it still has small scattering.

Next, we prove that a perfect invisibility effect can be

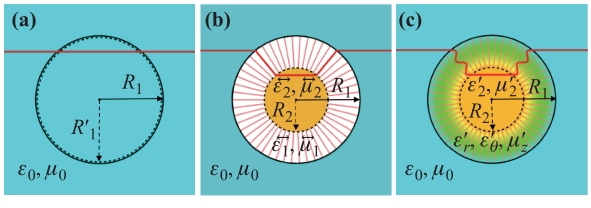

Fig. 1 Model of concentrator with simplified material parameters. Virtual space **(a)** and physical space **(b)** of concentrator from transformation optics. Physical space **(c)** with simplified material parameters.

obtained with the following parameters:

$$(\varepsilon_r', \varepsilon_\theta', \mu_z') = (\infty, 1, (R_1/r)^2). \tag{5}$$

Correspondingly, (ε_2', μ_2') are set as $(1, (R_1/R_2)^2)$. We call this situation the Perfect Case for emphasis. The effective refractive index of the inner region is R_1/R_2. The additional optical path along the r direction is

$$s = 2\int_{R_2}^{R_1} n(r)\mathrm{d}r = 2\int_{R_2}^{R_1} \frac{R_1}{r}\mathrm{d}r = 2R_1 \ln(R_1/R_2), \tag{6}$$

where "2" indicates that light rays cross the region between radii R_1 and R_2 twice. We consider Maxwell's equations at a fixed frequency ω in this Perfect Case, which is described as

$$\nabla \times \boldsymbol{E} = \mathrm{i}\omega\mu_0 \overleftrightarrow{\mu}\, \boldsymbol{H}, \tag{7}$$

$$\nabla \times \boldsymbol{H} = -\mathrm{i}\omega\varepsilon_0 \overleftrightarrow{\varepsilon}\, \boldsymbol{E}, \tag{8}$$

where ε_0 and μ_0 are the permittivity and permeability of vacuum, and $\overleftrightarrow{\varepsilon}$ and $\overleftrightarrow{\mu}$ are relative permittivity and permeability tensors of materials. In the region outside radius R_1 and inside radius R_2, the parameters of the materials are homogeneous. For the TM mode (E_r, E_θ, H_z), Maxwell's equations can be transformed into a Helmholtz equation, as follows:

$$\nabla^2 H_z + k_0^2 n^2 H_z = 0, \tag{9}$$

where k_0 is the wave vector satisfying $k_0^2 = \omega^2\varepsilon_0\mu_0$, and n is the effective refractive index. Therefore, the magnetic field can be expressed via the superposition of the Bessel function and Hankel function of the first kind [24]:

$$H_z(r) = \begin{cases} \sum_{m=-\infty}^{\infty} [\alpha_m J_m(k_0 r) + \beta_m H_m^1(k_0 r)]\mathrm{e}^{\mathrm{i}m\theta}, & r > R_1, \\ \sum_{m=-\infty}^{\infty} \gamma_m J_m(k_0 R_1/R_2 r)\mathrm{e}^{\mathrm{i}m\theta}, & r < R_2. \end{cases} \tag{10}$$

For the region between radii R_1 and R_2, Eqs. (7) and (8) can be expressed in a cylindrical coordinate system:

$$\frac{1}{r}\frac{\partial(rE_\theta)}{\partial r}\hat{z} = -\mathrm{i}\omega\mu_0\mu_z' H_z \hat{z}, \tag{11}$$

$$\frac{1}{r}\frac{\partial H_z}{\partial \theta}\hat{r} - \frac{\partial H_z}{\partial r}\hat{\theta} = \mathrm{i}\omega\varepsilon_0\varepsilon_r' E_r \hat{r} + \mathrm{i}\omega\varepsilon_0\varepsilon_\theta' E_\theta \hat{\theta}, \tag{12}$$

From Eq. (11) and (12), we obtain the following:

$$E_r = \frac{1}{\mathrm{i}\omega\varepsilon_0\varepsilon_r'}\frac{\partial H_z}{r\partial\theta}, \tag{13}$$

$$E_\theta = -\frac{1}{\mathrm{i}\omega\varepsilon_0\varepsilon_\theta'}\frac{\partial H_z}{\partial r}. \tag{14}$$

Since $\varepsilon_r' = \infty$, we obtain $E_r = 0$. After substituting Eq. (14) into Eq. (11), we obtain

$$\frac{\partial}{\partial r}\left(\frac{r}{\varepsilon_\theta'}\frac{\partial H_z}{\partial r}\right) + k_0^2 r\mu_z' H_z = 0. \tag{15}$$

According to the condition of Eq. (5), we can write

$$\frac{\partial}{\partial \ln(r)}\left(\frac{\partial H_z}{\partial \ln(r)}\right) + (k_0 R_1)^2 H_z = 0. \tag{16}$$

The solution of Eq. (16) can be expressed as

$$H_z(r) = c_1 \mathrm{e}^{\mathrm{i}k_0 R_1 \ln(r/R_2)} + c_2 \mathrm{e}^{-\mathrm{i}k_0 R_1 \ln(r/R_2)}, \tag{17}$$

where c_1 and c_2 are coefficients to be determined. We can express the magnetic field in this region in series form, similar to Eq. (10):

$$H_z(r) = \sum_{m=-\infty}^{\infty} [h_{1m}\mathrm{e}^{\mathrm{i}k_0 R_1 \ln(r/R_2)} + h_{2m}\mathrm{e}^{-\mathrm{i}k_0 R_1 \ln(r/R_2)}]\mathrm{e}^{\mathrm{i}m\theta}, \quad R_2 \le r \le R_1. \tag{18}$$

Thus, we obtain the form of the magnetic field in Fig. 1(c) for the Perfect Case, as shown in Eqs. (9) and (16). To determine the coefficients of these expressions, we further explore the continuous condition of H_z and E_θ. According to Eqs. (10), (14), and (18), we obtain four boundary conditions at radii R_1 and R_2 for each order of m:

$$\begin{cases} \alpha_m J_m(k_0 R_1) + \beta_m H_m^1(k_0 R_1) = h_{1m}\mathrm{e}^{\mathrm{i}k_0 R_1 \ln(R_1/R_2)} + h_{2m}\mathrm{e}^{-\mathrm{i}k_0 R_1 \ln(R_1/R_2)}, \\ \alpha_m J_m'(k_0 R_1) + \beta_m H_m^{1'}(k_0 R_1) = \mathrm{i}R_2[h_{1m}\mathrm{e}^{\mathrm{i}k_0 R_1 \ln(R_1/R_2)} - h_{2m}\mathrm{e}^{-\mathrm{i}k_0 R_1 \ln(R_1/R_2)}], \\ \gamma_m J_m(k_0 R_1) = h_{1m}\mathrm{e}^{\mathrm{i}k_0 R_1 \ln(R_1/R_2)} + h_{2m}\mathrm{e}^{-\mathrm{i}k_0 R_1 \ln(R_1/R_2)}, \\ \gamma_m J_m'(k_0 R_1) = \mathrm{i}R_2[h_{1m}\mathrm{e}^{\mathrm{i}k_0 R_1 \ln(R_1/R_2)} - h_{2m}\mathrm{e}^{-\mathrm{i}k_0 R_1 \ln(R_1/R_2)}]. \end{cases} \tag{19}$$

Suppose that the optical path of Eq. (6) and the wavelength satisfy the FPs [18]:

$$s = N\frac{2\pi}{k_0}, \tag{20}$$

where N is a positive integer. By substituting Eq. (20) into Eq. (19), we obtain

$$\begin{cases} \alpha_m J_m(k_0R_1) + \beta_m H_m^1(k_0R_1) = h_{1m}\mathrm{e}^{\mathrm{i}N\pi} + h_{2m}\mathrm{e}^{-\mathrm{i}N\pi}, \\ \alpha_m J_m'(k_0R_1) + \beta_m H_m^{1'}(k_0R_1) = \mathrm{i}R_2(h_{1m}\mathrm{e}^{\mathrm{i}N\pi} - h_{2m}\mathrm{e}^{-\mathrm{i}N\pi}), \\ \gamma_m J_m(k_0R_1) = h_{1m} + h_{2m}, \\ \gamma_m J_m'(k_0R_1) = \mathrm{i}R_2(h_{1m} - h_{2m}). \end{cases} \tag{21}$$

Thus, we obtain $\beta_m = 0, \gamma_m = \mathrm{e}^{\mathrm{i}N\pi}\alpha_m$, which means that there is no scattering wave outside radius R_1 and that the magnetic field has the same amplitude both outside radius R_1 and inside radius R_2. We analytically solve the magnetic field with simplified material parameters [Eq. (5)] at FPs [Eq. (20)]. In the following calculation, we use m ranging from -60 to 60 as a truncation and set $R_1 = 2$ and $R_2 = 1$ (A.U.). $\alpha_m = \mathrm{i}^m$. The real part and absolute value of the magnetic field under an incident plane wave with $\alpha_m = \mathrm{i}^m$ are plotted in Figs. 2(a) and (b), respectively. We also show the numerical simulations of such a device in Figs. 2(c) and (d) under the same condition as Figs. 2(a) and (b), which are obtained using Comsol Multiphysics. The analytical solution and numerical simulation are consistent with each other and demonstrate the perfect invisibility.

We also show that the invisibility effect can be obtained in the other two parameters. Although the invisibility effect is not perfect, it is quite good (in a sense, almost perfect). Moreover, the amplitude of the magnetic field inside radius R_2 can be controlled by choosing different parameters. In one such case, which we call Case

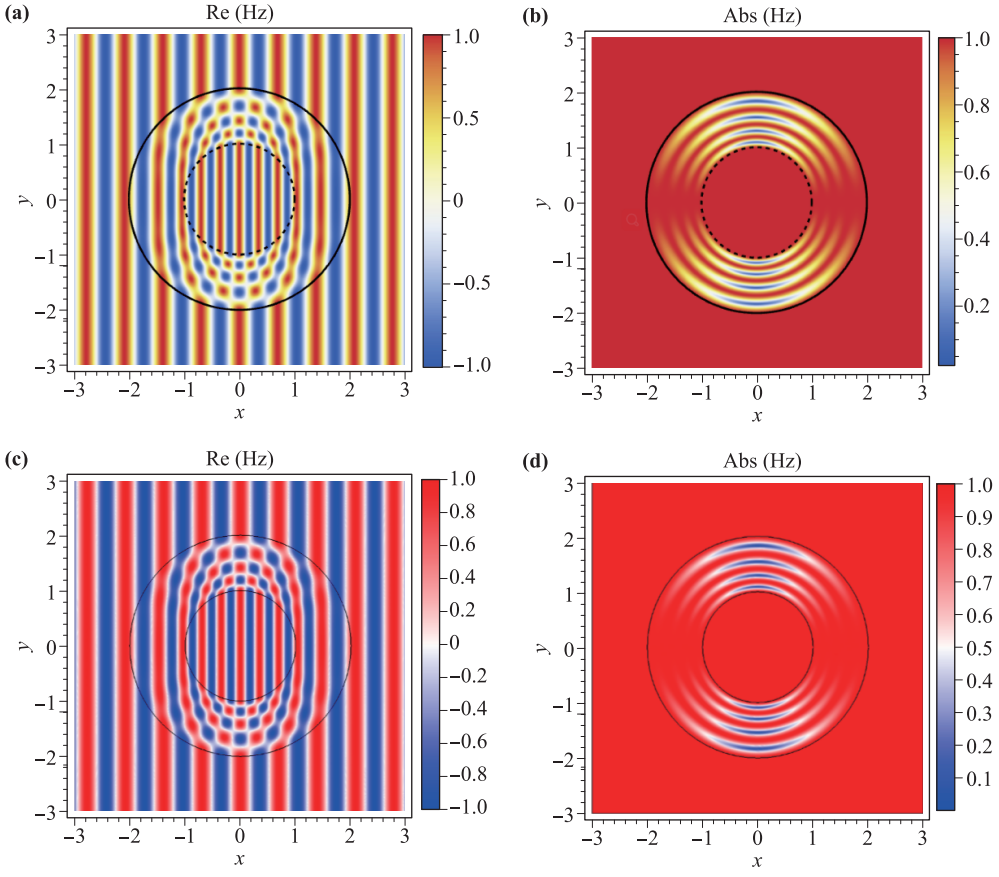

Fig. 2 Fields of concentrator in Perfect Case. Analytical calculation: **(a)** Real part of magnetic field. **(b)** Absolute value of magnetic field. Numerical simulation: **(c)** Real part of magnetic field. **(d)** Absolute value of magnetic field.

A,

$$(\varepsilon'_r, \varepsilon'_\theta, \mu'_z) = (\infty, r/R_1, (R_1/r)^3), \tag{22}$$

and (ε'_2, μ'_2) are $(R_2/R_1, (R_1/R_2)^3)$.

In the other case, which we call Case B,

$$(\varepsilon'_r, \varepsilon'_\theta, \mu'_z) = (\infty, (R_1/r)^2, 1), \tag{23}$$

and (ε'_2, μ'_2) are $((R_1/R_2)^2, 1)$. After performing the aforementioned procedure, we can obtain almost perfect invisibility if the wavelength of the incident wave satisfies FPs, as shown in Eq. (20).

For Case A, with the incident plane wave, the real part and absolute value of the magnetic field are analytically solved using the aforementioned method. These field patterns are plotted in Figs. S1(a) and (b), respectively, of the Supplementary Material. The amplitude of the magnetic field inside radius R_2 is almost half of that outside radius R_1 ($R_1 = 2$ and $R_2 = 1$). Importantly, the scattering coefficient β_m is no longer zero, although it is very small. The absolute value of the scattering magnetic field is shown in Fig. S1(c). Compared with Fig. S1(b), the scattering magnetic field can be almost neglected, which indicates almost perfect invisibility in this case. Correspondingly, the numerical simulations shown in Figs. S1(d)–(f) are consistent with the analytical calculations in Figs. S1(a)–(c).

For Case B, the real part and absolute value of the magnetic field are plotted in Figs. S2(a) and (b), respectively. The amplitude of the magnetic field inside radius R_2 is approximately twice of that outside radius R_1 ($R_1 = 2$ and $R_2 = 1$), which differs from Case A. The scattering coefficients β_m are also nonzero but very small. The absolute value of the scattering magnetic field in Fig. S2(c) is larger than that of Case A. However, it can be neglected when compared with the incident wave. The corresponding numerical simulations are shown in Figs. S2(d)–(f). The permeability of the whole device is μ_0, which exhibits no change under a magnetic field. Therefore, this invisibility concentrator can be realized with a pure dielectric profile.

To further demonstrate the invisibility effect of these three cases, their scattering cross sections σ are plotted in Fig. 3. Herein, the scattering cross section is defined as the sum over all the squares of the absolute values of the scattering coefficients:

$$\sigma = \sum_{m=-\infty}^{\infty} |\beta_m|^2. \tag{24}$$

In our calculation, we use m ranging from -60 to 60 as a truncation, which results in a good asymptotic value of the real scattering cross section. The x-axis of Fig. 3 denotes the wave number from Eqs. (6) and (20):

$$k = \frac{s\omega}{2\pi c}. \tag{25}$$

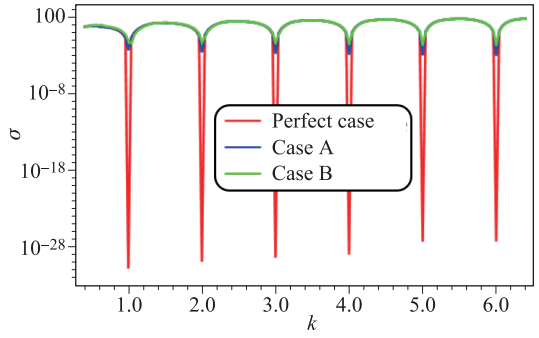

Fig. 3 Scattering cross-section of the above three cases.

As shown in Fig. 3, the needle tips at integer values of k indicate that the scattering is very small, i.e., the invisibility effect of these devices occurs at the FPs. For the Perfect Case, the value of the scattering coefficients at the FPs are small enough to prove the existence of perfect invisibility. The invisibility performance of Case A is better than that of Case B.

The aforementioned cases demonstrate that the magnetic fields inside and outside the device are almost uniform. Therefore, we define a parameter D to represent the ratio between the average absolute value of the magnetic field inside and outside:

$$D = \frac{\langle Abs(H_z)\rangle_{inside}}{\langle Abs(H_z)\rangle_{outside}}. \tag{26}$$

We numerically find that the parameter D is of the form

$$D = \sqrt{\varepsilon'_2} = \frac{R_1}{R_2\sqrt{\mu'_2}}, \tag{27}$$

as shown in Fig. 4. Owing to the concentration effect of our design, the energy in the region inside radius R_1 can be compressed into the region inside radius R_2. By choosing simplified material parameters, we can tune (ε'_2, μ'_2) to freely control the amplitude of the magnetic field.

In conclusion, we present a series of invisibility devices with simplified material parameters beyond TO. One of

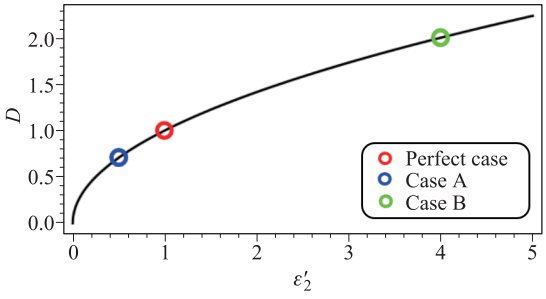

Fig. 4 The parameter D as a function of ε'_2 of the inner core.

them can achieve the perfect invisible effect at frequencies of FPs, while the others have very small scattering. We can also freely tune the amplitude of the magnetic field inside the device by choosing simplified material parameters. The required materials are feasible in practice. Case B can be achieved even with a pure dielectric profile. Analytical calculation and numerical simulation confirm the functionalities of these devices. To realize such invisibility devices, we can construct a gradient dielectric separation via a thin metal slit, which was used for reduced concentrators in Ref. [18]. Moreover, if we consider the (H_r, H_θ, E_z) mode and only focus on the parameters of $(\mu_r', \mu_\theta', \varepsilon_z')$, the above results are still valid. However, perfect magnetic conductors must be used during the implementations.

Electronic supplementary material Supplementary material is available in the online version of this article at https://doi.org/10.1007/s11467-018-0764-4 and is accessible for authorized users.

Acknowledgements This work was supported by the Fundamental Research Funds for the Central Universities (grant No. 20720170015) and the National Science Foundation of China for Excellent Young Scientists (grant No. 61322504). M. Z. and L. X. contributed equally to this work.

References

1. U. Leonhardt, Optical conformal mapping, *Science* 312(5781), 1777 (2006)
2. J. B. Pendry, D. Schurig, and D. R. Smith, Controlling electromagnetic fields, *Science* 312(5781), 1780 (2006)
3. E. J. Post, Formal Structure of Electromagnetics: General Covariance and Electromagnetics, Courier Corporation, 1997
4. U. Leonhardt and Philbin, T, Geometry and Light: The Science of Invisibility, New York: Dover Inc., 2010
5. U. Leonhardt and T. G. Philbin, General relativity in electrical engineering, *New J. Phys.* 8(10), 247 (2006)
6. H. Chen and C. Chan, Transformation media that rotate electromagnetic fields, *Appl. Phys. Lett.* 90(24), 241105 (2007)
7. J. Li and J. Pendry, Hiding under the carpet: A new strategy for cloaking, *Phys. Rev. Lett.* 101(20), 203901 (2008)
8. C. Chu, X. Zhai, C. J. Lee, P.H. Wang, Y. Duan, D. P. Tsai, B. Zhang, and Y. Luo, Phase-preserved macroscopic visible-light carpet cloaking beyond two dimensions, *Laser Photonics Rev.* 9(4), 399 (2015)
9. Y. Lai, H. Chen, Z. Q. Zhang, and C. T. Chan, Complementary media invisibility cloak that cloaks objects at a distance outside the cloaking shell, *Phys. Rev. Lett.* 102(9), 093901 (2009)
10. Y. Lai, J. Ng, H. Chen, D. Z. Han, J. J. Xiao, Z.Q. Zhang, and C. T. Chan, Illusion optics: The optical transformation of an object into another object, *Phys. Rev. Lett.* 102(25), 253902 (2009)
11. T. Y. Huang, H. C. Lee, I. W. Un, and T. J. Yen, An innovative cloak enables arbitrary multi-objects hidden with visions and movements, *Appl. Phys. Lett.* 101, 151901 (2012)
12. M. Rahm, D. Schurig, D. A. Roberts, S. A. Cummer, D. R. Smith, and J. B. Pendry, Design of electromagnetic cloaks and concentrators using form-invariant coordinate transformations of Maxwell's equations, *Photon. Nanostructures* 6(1), 87 (2008)
13. M. M. Sadeghi, H. Nadgaran, and H. Chen, Perfect field concentrator using zero index metamaterials and perfect electric conductors, *Front. Phys.* 9, 90 (2014)
14. D. Schurig, J. Mock, B. Justice, S. A. Cummer, J. B. Pendry, A. F. Starr, and D. R. Smith, Metamaterial electromagnetic cloak at microwave frequencies, *Science* 314(5801), 977 (2006)
15. H. Chen, B. Hou, S. Chen, X. Ao, W. Wen, and C. T. Chan, Design and experimental realization of a broadband transformation media field rotator at microwave frequencies, *Phys. Rev. Lett.* 102(18), 183903 (2009)
16. M. Yan, Z. Ruan, and M. Qiu, Cylindrical invisibility cloak with simplified material parameters is inherently visible, *Phys. Rev. Lett.* 99(23), 233901 (2007)
17. W. Yan, M. Yan, and M. Qiu, Generalized compensated bilayer structure from the transformation optics perspective, *J. Opt. Soc. Am. B* 26(12), B39 (2009)
18. M. M. Sadeghi, S. Li, L. Xu, B. Hou, and H. Chen, Transformation optics with Fabry-Pérot resonances, *Sci. Rep.* 5(1), 8680 (2015)
19. C. Navau, J. Prat-Camps, O. Romero-Isart, J. I. Cirac, and A. Sanchez, Long-distance transfer and routing of static magnetic fields, *Phys. Rev. Lett.* 112(25), 253901 (2014)
20. F. Sun and S. He, DC magnetic concentrator and omnidirectional cascaded cloak by using only one or two homogeneous anisotropic materials of positive permeability, *Prog. Electromagnetics Res.* 142, 683 (2013)
21. J. Prat-Camps, C. Navau, and A. Sanchez, Experimental realization of magnetic energy concentration and transmission at a distance by metamaterials, *Appl. Phys. Lett.* 105(23), 234101 (2014)
22. C. Navau, J. Prat-Camps, and A. Sanchez, Magnetic energy harvesting and concentration at a distance by transformation optics, *Phys. Rev. Lett.* 109(26), 263903 (2012)
23. F. Sun and S. He, Transformation inside a Null-space region and a DC magnetic funnel for achieving an enhanced magnetic flux with a large gradient, *Prog. Electromagnetics Res.* 146, 143 (2014)
24. H. C. van de Hulst, Light Scattering by Small Particles, Courier Corporation, 1957